

THERMAL PERFORMANCE MODELING OF A NOVEL DUAL-PCM EVACUATED
U-TUBE SOLAR COLLECTOR

A THESIS
IN
Mechanical Engineering

Presented to the Faculty of the University
of Missouri–Kansas City in partial fulfillment of
the requirements for the degree

MASTER OF SCIENCE

by
CELINE S.L. LIM

B. S., University of Missouri-Kansas City, 2019

Kansas City, Missouri
2020

© 2020
CELINE S.L. LIM
ALL RIGHTS RESERVED

THERMAL PERFORMANCE MODELING OF A NOVEL DUAL-PCM EVACUATED
U-TUBE SOLAR COLLECTOR

Celine S.L. Lim, Candidate for the Master of Science Degree
University of Missouri–Kansas City, 2020

ABSTRACT

Solar water heating (SWH) systems are a well-established and eco-friendly way to generate hot water for household or commercial applications as it utilizes energy from solar radiation which is readily available all year round. However, there are drawbacks to this technology especially during times where solar intensity is inconsistent. To overcome this drawback, a backup booster unit is often required to power the SWH system. Recent studies have shown that utilizing phase change material (PCM) as an energy storage medium in SWH systems can alleviate the effect the booster unit. Nevertheless, current SWH technology has the PCM-based storage unit designed as a separate medium away from the solar collectors. The novelty of this study lies in the design of a new SWH that combines heat transfer and storage both in a single unit as well as the study of PCM as a heat transfer fluid (HTF). The selected type of collector for this purpose is an evacuated tube solar collector (ETC) and the new design of a dual-PCM evacuated u-tube collector

(EUTC) has been developed by applying a U-tube inside the collector which contains the HTF. The solid-liquid PCM, Trtriacontane paraffin ($C_{33}H_{68}$), was integrated inside the dual-PCM EUTC for direct heat storage on the system and delayed release of heat.

Thermal analysis was first conducted to investigate the appropriate PCM as a HTF, in which HITEC molten salt and erythritol ($C_4H_{10}O_4$) was chosen. This study also analyzes PCM doped with nanoparticles to be used as HTFs directly integrated in the dual-PCM EUTC. Preliminary analysis showed that erythritol would be a better combination as a HTF in moderating operating temperature conditions (150°C) of this system due to its high specific heat capacity in liquid form, as well as its unique sub-cooling behavior. In order to overcome the low thermal conductivity of erythritol and further enhance specific heat capacity, a weight concentration of 1% multi-walled carbon-nanotubes (MWCNT) is added. Additionally, to insure even distribution of MWCNT and consistent properties of the HTF, triethanolamine (TEA) is proposed to be incorporated as a dispersant. Thermal analysis tests show 12.4% enhancement of specific heat capacity of the proposed HTF mixture as well as nearly 5°C depression of freezing onset temperature.

Subsequently, a computational fluid dynamics (CFD) modeling of a single U-tube ETC is performed using ANSYS Fluent in stagnation (on-demand) operation. A 3D model of the ETC is developed and the appropriate boundary conditions was applied. The thermal performance comparison of the dual-PCM EUTC with erythritol as a HTF vs commercially available heat pipe ETC has been done. Simulation results shows a

maximum fin temperature difference up to 24°C enhancement of the dual-PCM EUTC compared with heat pipe ETC. A comparison of several different types of HTFs was also investigated in the new dual-PCM EUTC system. From this analysis, it can be predicted that the erythritol+MWCNT+TEA provides more hot water to the demand side.

APPROVAL PAGE

The faculty listed below, appointed by the Dean of the School of Computing and Engineering, have examined a thesis titled “Thermal Performance Modeling of a Novel Dual-PCM Evacuated U-Tube Solar Collector,” presented by Celine S.L. Lim, candidate for the Master of Science degree, and hereby certify that in their opinion it is worthy of acceptance.

Supervisory Committee

Sarvenaz Sobhansarbandi, Ph.D., Committee Chair
Department of Civil & Mechanical Engineering

Gregory King, Ph.D., P.E.
Department of Civil & Mechanical Engineering

Zahra Niroobakhsh, Ph.D.
Department of Civil & Mechanical Engineering

CONTENTS

ABSTRACT	iii
ILLUSTRATIONS	ix
TABLES	x
ACKNOWLEDGEMENTS	xi
Chapter	
1 INTRODUCTION	1
2 THERMAL ANALYSIS OF PHASE CHANGE MATERIAL AS A HEAT TRANS- FER FLUID	11
2.1 PCM as Latent Heat Storage	13
2.2 HITEC Molten Salt as HTF	14
2.3 Erythritol as HTF	18
2.4 Erythritol + 1%MWCNT + TEA as HTF	19
2.5 Comparison of HITEC Salt and Erythritol as HTF	21
3 DESIGN AND MODELING OF AN EVACUATED U-TUBE COLLECTOR INTEGRATED WITH DUAL-PCM CONFIGURATION	23
3.1 System Configuration	23
3.2 Computational Fluid Dynamics Modeling	24
4 CFD RESULTS AND DISCUSSION	35
4.1 Comparison of Heat Pipe ETC and Dual-PCM EUTC Performance	35

4.2 Comparison of Different HTF in dual-PCM EUTC	39
5 CONCLUSION	42
6 FUTURE WORK	45
APPENDIX	
A INSTRUMENT PARAMETERS	46
REFERENCE LIST	47
VITA	57

ILLUSTRATIONS

Figure		Page
1	Types of Thermal Energy Storage [50]	3
2	Heat Flow versus Time of Pure HITEC Salt (Averaged across three samples)	16
3	Heat Flow versus Time of Erythritol (Averaged across three samples) . . .	19
4	Schematic of the dual-PCM EUTC SWH System	24
5	U-Tube ETC Geometry	25
6	Meshing from Isometric and Cross-section View of U-Tube ETC	29
7	Meshing from Top and Bottom View of U-Tube ETC	30
8	User Defined Functions (Temperature Profile)	32
9	Fin Temperature Inside ETC versus Time	36
10	Liquid Fraction of PCM72 Inside ETC versus Time	37
11	Fin Temperature Using Different HTF Inside ETC versus Time	39

TABLES

Tables		Page
1	Properties of Selected Nanoparticles [26, 60]	15
2	Thermophysical Properties of Pure HITEC and HITEC + Nanoparticles .	17
3	Thermophysical Properties of Pure Erythritol	20
4	Erythritol Melting/freezing and Specific Heat Capacity Comparison . . .	21
5	Specification of U-Tube Integrated ETC [15, 39, 41].	26
6	Thermophysical Properties Latent Heat Storage PCM72 [34]	27
7	Thermophysical Properties of Selected HTF [21, 25, 29, 40, 48]	28
A.1	TGA5500 Instrument Specification	46
A.2	DSC2500 Instrument Specification	46

ACKNOWLEDGEMENTS

First and foremost I would like to thank my advisor, Dr Sarvenaz Sobhansarbandi, for being a reliable mentor, support, and guidance throughout the process of completing this thesis. Special thank you to my lab mates; Tyler O'Neil, Vivek Pawar, Jordan Berg, and Arman Nokhosteen for you all have worked with me throughout the time of my thesis and have been nothing but an amazing support during times when I thought it was impossible. I would also like to thank my thesis committee members, Dr Gregory King and Dr Zahra Niroobakhsh for taking time to be apart of this journey. Last but not least, I would like to thank my friends and my family, my dad and my mom, for their moral support from 10,000 miles away. Without them none of this would have been possible.

CHAPTER 1

INTRODUCTION

Solar water heating (SWH) systems are an eco-friendly, cost-effective and a sustainable way to generate hot water for household or commercial applications as it utilizes solar radiation which is readily available all year round. The main component of a SWH is a solar collector which absorbs the radiation from the sun and subsequently transfers the heat collected to heat water on the demand side. Traditional solar collectors include flat-plate collectors (FPCs) and evacuated tube collectors (ETCs). While FPCs are more commonly used in household SWH systems, the design of FPCs are significantly more disadvantageous compared to ETCs due to its fixed-position and inability to track the position of sun throughout the day [30]. ETCs are also designed to be stronger and longer lasting, and if one evacuated tube breaks it is inexpensive to replace a single tube unlike FPCs which requires replacement of the whole panel [35]. Besides, the ETCs are gaining more attention as they are more efficient compared to other types of solar collectors due to a vacuum region that prevents convective heat loss from the interior of ETC to the surrounding as well as its cylindrical geometry which allows for passive tracking of the sun [45]. Additionally, ETCs are often more desirable due to its high efficiency especially in higher operating temperature conditions as well as being economically advantageous compared to other types of commercially available solar collectors [44]. Sakhrieh et.al

inspected and compared 5 different types of solar collectors in terms of overall performance, quality, payback period, and maintenance follow-up, where the authors found that the ETC has the highest efficiency among all with a satisfactory payback period [46]. A comprehensive study by Sabiha et.al on the progress and development of ETCs also showed that ETCs are efficient in higher operating temperature conditions as well as being cost effective when used in cold-weather countries [45].

ETCs can also be further categorized into different types such as the Heat pipe ETC (HPETC) and U-pipe (or also known as U-tube) ETC [45]. The important part of HPETC is the thermosyphon heat pipe that uses water or ethylene-glycol as a working fluid [5, 39]. The heat pipe transfers the heat collected from the sun up to the manifold, where cold water passes through. The working concept of a thermosyphon heat pipe is based on the evaporation/condensation phenomena of a small droplet of working fluid inside the heat pipe, where when heated the working fluid evaporates to the top of the heat pipe and as it condenses gravity pulls it back to the bottom [5]. Meanwhile, the U-tube ETC was developed to further improve upon the disadvantages of an all-glass ETC, where the U-tube ETC was reported to have the ability to attain higher temperature, has longer service life, and has the ability to withstand higher pressure [20]. Unlike the HPETC where the HTF is permanently situated inside the heat pipe, the U-tube ETC configuration often have the HTF runs through the whole system where the HTF gets heated up as it travels down the the copper U-tubes inside the ETCs.

To improve the functionality and efficiency of SWH systems, the use of thermal energy storage (TES) materials have been widely investigated. TES materials are used to

store excess heat collected throughout the day before releasing the stored heat back during peak/on-demand hours. It is a cheap and environmentally friendly energy management method that has the capability to reduce carbon footprints as well as reducing greenhouse gas emissions. TES can be classified into three different forms – sensible heat storage, latent heat storage, and thermo-chemical storage as seen in Figure 1. For residential SWH systems, sensible and latent heat storage methods are more applicable as thermo-chemical storage technology are generally incorporated into larger power plant such as the concentrating solar power (CSP) systems and are currently still in early laboratory development stages [3, 43]. Sensible heat storage can be defined as energy storage associated with change in temperature without any phase change. Meanwhile, latent heat storage is the energy storage associated with phase change of a material.

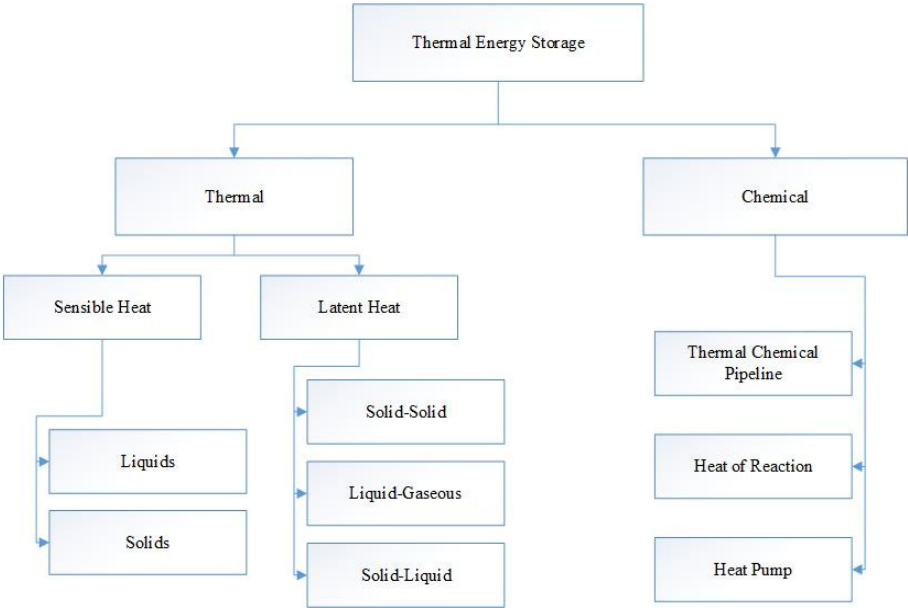


Figure 1: Types of Thermal Energy Storage [50]

Phase change material (PCM) is a common type of latent heat storage material

used in SWH systems that have been gaining attention due to its ability to absorb and store large quantity of heat to be used at a later time through the phase change process. PCMs can be classified into organic, inorganic, and eutectic materials where many studies have been conducted regarding PCMs and thermal energy storage systems in an effort to increase the efficiency of solar energy technology for industrial/domestic and building applications [6, 8, 9, 61]. Absi et. al studied the usage of PCM on external surface of buildings and found that PCMs have the potential to reduce the problem of overheating of buildings due to direct solar radiation in Malaysia [1]. Besides building applications, an innovative method of using PCMs to maintain thermal comfort level for a passenger vehicle in which Saleel et. al investigated the use of coconut oil as PCM to to reduce cabin temperature during the day [47]. Paraffin wax is a popular type of organic PCM that has outstanding latent heat properties and can be categorized into two broad ranges based on its melting temperature – high melting temperature over 100°C and low melting temperature below 100°C. Paraffin waxes also have stable chemical/physical properties as they are non-toxic, non-hazardous, inexpensive, and are widely available, which makes them a feasible option for thermal energy storage applications. More research have been done in recent years on the use of paraffin wax PCM in conjunction with solar collectors to increase the efficiency of SWH systems [32]. Fazilati et.al proposed integrating encapsulated paraffin wax with a melting temperature of 55°C into the system's jacketed shell tank (heat exchanger) [16]. The proposed configuration resulted in up to 25% of extended time in hot water supply. Besides, Papamidros et. al studied a novel method of integration of PCMs into ETCs, where the study showed significant improvement of the systems'

functionality during on-demand operation where solar intensity is insufficient [39].

Large-scale solar power plants such as the concentrating solar power (CSP) systems often utilize molten salts with high melting point and high thermal stability as a HTF [49, 62]. Common molten salts used are the HITEC molten salt, which is a ternary eutectic salt mixture with weight percentage composition of 53% KNO_3 , 40% NaNO_2 and 7% NaNO_3 and Solar Salts which are composed of 60% NaNO_3 and 40% KNO_3 . HITEC salt have been receiving more attention due to its much lower melting point of 142°C when compared to Solar Salts that has melting temperature of 220°C , is thermally stable up to a very high temperature of 500°C , have high thermal conductivity, and high specific heat capacity [42, 62]. Nevertheless, many research efforts have been focused on the enhancement of thermophysical properties of HITEC salts through the addition of nanoparticles. Ho et. al doped HITEC salts with different weight compositions (between 0.016 wt.% to 2 wt.%) of alumina (Al_2O_3) nanoparticles and found that 0.063 wt.% of Al_2O_3 nanoparticle addition yields up to 19.9% increase in specific heat capacity [24]. Chieruzzi et. al investigated a several different types of nanoparticles such as Al_2O_3 , titania (TiO_2), silica (SiO_2), and a combination of SiO_2 - Al_2O_3 to be added into the base salt mixture of Solar Salt (60% NaNO_3 :40% KNO_3) [11]. The authors found that the addition of a 1 wt.% of nanoparticles have the ability to enhance specific heat capacity of the base salt mixture by 15% to 57% in solid phase and by 1% to 22% in liquid phase, making the selected nanoparticles studied attractive for this current study. Furthermore, several researchers have also studied the effect of multi-walled carbon nanotubes (MWCNT) on molten salts. Hamdy et. al found that the addition of 0.1% of MWCNT to solar salts leads

to an increase in latent heat of fusion by approximately 36% along with an enhancement in thermal conductivity of up to 50% as the amount of MWCNT added increases up to 1.5% [22]. Meanwhile, Wu et. al found that by doping MWCNT into solar salts melting point depression of solar salts can be observed and an impressive increase in thermal conductivity of 293% was demonstrated [65].

Erythritol, a type of non-toxic sugar sweetener (or sugar alcohol) that can often be found in a kitchen of a regular household, is also another common type of PCM used as a thermal energy storage material for medium to high operating temperature ranges ($\sim 150^{\circ}\text{C}$) [38, 51, 64]. Erythritol have been widely investigated as a PCM due to its desirable properties. For example, erythritol has high latent heat properties, exceptional specific heat capacity when compared to paraffin wax, non-toxic, and has good thermal conductivity properties on top of being inexpensive and as well as it can very easily be acquired [55,64]. A recent study from Anish et. al compared the performance of erythritol and xylitol in a heat exchanger and found that erythritol showed superior charging effect as a PCM [4]. Another application of PCM-based erythritol was studied by Coccia et. al where the authors proposed inserting erythritol into a solar box cooker [12]. However, the disadvantage of erythritol as a thermal energy storage material is due to its drastic sub-cooling behavior that leads to the reduction in heat released back into the system during the crystallization phase (from liquid to solid phase) [37, 63]. Furthermore, as erythritol crystallizes from liquid to solid form, the material goes through a significant volumetric expansion of approximately 14% [33]. In this research, this sub-cooling effect can actually be seen as an advantage when investigating erythritol as a heat transfer fluid

(HTF) where the sub-cooling effect of erythritol allows for erythritol to maintain in liquid form for a longer period of time before crystallizing. Moreover, erythritol has a higher melting temperature compared to traditional HTFs such as water and glycol. This high melting point of erythritol is also a desirable property as a HTF as it will hold more heat, and hence heating domestic water up to a higher temperature and providing more hot water for household or commercial activities.

As a PCM, the investigation of erythritol doped with nanoparticles have been widely investigated to improve its thermal conductivity properties, which can also be implemented when examining erythritol as a HTF. Zeng et. al [66] found that the addition of 0.1% volume fraction of MWCNT into silica nanospheres improved its thermal conductivity by approximately 7%. Another research from Shen et. al also found that 1% of MWCNT when dispersed in erythritol greatly enhances the thermal conductivity of erythritol [52]. Although research shows positive effects from inclusion of nanoparticles, reliability of these effects depends on stability of a homogenous mixture. The use of dispersants has shown to improve the stability and homogeneity of nanoparticle-doped erythritol mixtures. Zhichao et. al [67] determined triethanolamine (TEA) when used as a dispersant at roughly 50% weight of added nano-titania nanoparticles yields the best results for stability and specific heat enhancement of erythritol based PCM. Based on literature review, TEA was then chosen as a dispersant to be used in erythritol with MWCNT nanoparticles where TEA was incorporated at 0.5 wt.% for total sample weight. The effects on specific heat capacity, and melting behavior from incorporating MWCNT in erythritol HTF with and without TEA dispersant was then investigated.

For comparison purposes in this study, traditional HTFs such as ethylene-glycol was selected as a HTF in the U-tube ETC system as it has a high boiling point of 197°C, high thermal conductivity, and high specific heat capacity [10]. It is important to note that ethylene-glycol is not a type of PCM. Ethylene-glycol are often mixed with pure water (EG/PW) in different composition to form a HTF mixture to further enhance the HTFs specific heat capacity and thermal conductivity [31, 56]. However, for a medium-high operating temperature U-tube ETC system, EG/PW HTFs are not desirable as they have a lower boiling point of approximately 107°C [10]. Besides ethylene-glycol, silicone oil was also selected to be used as a HTF for comparison with erythritol. Unlike the HPETC where water can be used as the HTF inside a vacuumed thermosyphon heat pipe, using water as the HTF in a U-tube ETC with medium-high operating conditions could pose problems such as the evaporation of water at approximately 100°C which causes the HTF to lose energy. The evaporation of water subsequently causes the HTF to lose energy. Additionally, it could also cause an increase in pressure of the tubes which could potentially lead to issues relating to pumping effect of water HTF throughout the system.

Modern SWH technology has the PCM-based storage unit designed as a separate medium away from the solar collectors. This study proposes a novel dual-PCM system that combines the heat transfer and storage both in a single unit inside the U-tube ETC, in which the U-tube effectively replaces the thermosyphon heat pipe found in traditional ETCs. The selected type of energy storage material is Trtriacontane paraffin ($C_{33}H_{68}$),

while using erythritol ($C_4H_{10}O_4$) as HTF. The novelty of this study also lies in the investigation of erythritol as a HTF, which is still a fairly unexplored territory. Such configuration consequently replaces the effect of heat pipe with a U-tube in commercially available ETCs. The HTF with higher operating temperature will flow through the U-tube, which flows into an external heat exchanger that transfers heat to the water. The novelty of this study is the reduced rate of heat loss due to the vacuum layer, increased rate of energy storage by integrating dual-PCMs directly inside the tube, and finally enhanced rate of heat transfer by incorporating a HTF with high heat capacity. Selection of a suitable HTF is vital as it contributes to improving the efficiency of the system, consequently reduces the cost of operation.

Preliminary investigation on the proposed system was done using computational fluid dynamics (CFD) methods. CFD is a powerful, efficient, and cost effective optimization tool that solves complex fluid flow problems using numerical analysis [36]. CFD analysis is especially useful for initial design stages of a new system and are often utilized by academic researchers to model, evaluate, and optimize ETC based solar thermal systems [2, 7, 13, 27]. A computational fluid dynamics modeling of a heat pipe evacuated tube solar collector (HPETC) integrated with PCM was developed by Pawar et.al [41]. In the first part of said study, a 3D model of commercially available HPETC was simulated, while in the second part the HPETC integrated with the PCM was developed to analyze the improved thermal distribution. In spite of the temperature distribution inside the tube, melting fraction and its effect on performance the HPETC was also studied. The

simulation results showed acceptable agreement between the CFD modeling and the experimental data of the HPETC system. It was also found that the melting fraction of the PCM was reached up to 70% which can be further improved by enhancing thermal conductivity of the PCM by the addition of some high thermally conductive materials such as nanoparticles or by using porous medium inside the tube. The similar geographical and thermophysical properties of the materials, as well as appropriate boundary conditions are applied to the dual-PCM evacuated U-tube collector (dual-PCM EUTC) system proposed for this study. This modeling tool can serve as a preliminary benchmark for further optimization of the dual-PCM EUTC system.

In this research, two different scopes of experiment were conducted; the thermal analysis of PCMs as heat transfer fluid with addition of nanoparticles and the CFD analysis of the U-tube ETC using the selected HTF as a dual-PCM configuration. The proposed dual-PCM EUTC system was compared with the commercially available HPETC from previous experimental work by analyzing the discharging rate (releasing of latent heat energy) of the PCM and its effect on fin temperature from both systems in a stagnation (on-demand) operation. It is expected that the dual-PCM EUTC configuration will perform better in terms of maintaining higher fin temperature for a longer period of time than the commercially available HPETC with PCM integrated in the tubes.

CHAPTER 2

THERMAL ANALYSIS OF PHASE CHANGE MATERIAL AS A HEAT TRANSFER FLUID

For a medium operating temperature system, HTF that has higher melting temperature and higher specific heat capacity flows through a U-tube to replace the effect of heat pipe in commercially available ETCs was chosen. The thermal analysis of the selected HTFs are especially vital to understand the behaviour of the material as it undergoes a range of temperature. Two main instruments used when conducting thermal analysis of the selected HTFs are the Thermogravimetric Analysis (TGA) and the Differential Scanning Calorimetry (DSC).

The TGA measures the mass of the sample over time across a range of temperature. This is a crucial procedure to ensure that the sample does not decompose past 5 weight percent (wt%) of the initial sample weight at the specified range of temperature. Decomposition of the sample in the TGA past 5 wt% will potentially contaminate and damage the DSC, where critical thermophysical properties such as melting/crystallization onset temperature, latent heat, and specific heat capacity of the sample were measured in a modulated heating and cooling cycle. Besides contaminating the DSC, materials that decomposes in the specified range of operating temperature could damage the equipment used during experimental stage of this research.

The first step in the thermal analysis of the selected samples is by conducting a TGA test using the Discovery TGA5500 manufactured by TA Instruments. As the

TGA5500 has an internal balance, it is recommended by the manufacturer to always tare empty pans prior to loading the sample pans as by following this step guarantees the most accurate weight of the sample to be tested [58]. Following the TGA test, sample sizes of materials at approximately 10-15mg were prepared and hermetically sealed in a Tzero hermetic aluminum pan to be tested on the DSC. The DSC test was then conducted using the Discovery DSC2500, also manufactured by TA Instruments. The DSC measures properties of the sample by analyzing the temperature difference between an empty reference pan and a sample pan inside the same furnace under the same operating temperature conditions [57]. The DSC also runs tests in a modulated heating ramp in which the temperature oscillated during ramps as a sinusoidal wave, hence producing accurate specific heat capacity value [57]. Moreover, to obtain extra confidence in the DSC testing and to have better reliability of the results, repeatability tests were conducted where three samples of each mixture were prepared and tested. The results acquired were then averaged across all three samples. Furthermore, each sample were tested in two heat/cool cycles and data were extracted from the second heat/cool cycle. This is to ensure that the thermal history of the material resets and stabilized after the first heat/cool. Collecting data off the second heat/cool cycle also ensures that enthalpic recovery of the material takes places in which it reduces variation in data collected from the sample due to processing effects from a newly prepared sample [59]. All TGA tests were conducted using a heating ramp of 3°C/min.

To guarantee the accuracy of the instrument and to gain confidence with test results, four different types of calibration method were implemented preceding any testing

on the DSC. This includes the Tzero calibration, cell constant calibration, temperature calibration, and reversing heat capacity calibration [57]. These calibrations uses 99.99% pure materials for calibration such as sapphire (for heat capacity calibrations) and indium (for enthalpy and temperature calibrations). Furthermore, the furnace cell is cleaned and baseline verification tests are conducted regularly to verify that there are no contaminants in the furnace cell as well as to ensure that the DSC device yields minimal drift in results.

2.1 PCM as Latent Heat Storage

Previous studies on thermal analysis of paraffin wax was conducted by Lim et. al [34]. In that study, three different types of paraffin wax as PCM was analyzed: (octadecane) PCM28, (hexadecane) PCM58, and (tritriacontane) PCM72 where PCM28 and PCM58 tested is in microencapsulated form while PCM72 is in pellet form. Based on that study, PCM72 was selected to fill the ETC due to its high melting temperature, high thermal conductivity, and high latent heat capacity [34]. In addition, PCM72 was selected to be integrated in the ETC based on previous experimental work where the maximum averaged fin temperature achieved was observed to be approximately 100°C under normal operation [39]. This allows for PCM72 to be fully melted and hence, allows for maximum utilization of the latent heat storage properties for this system.

2.2 HITEC Molten Salt as HTF

Firstly, HITEC molten salts were selected for this study due to its lower melting temperature when compared to other types of molten salt, its high thermal conductivity, high specific heat capacity, and its low viscosity [62]. In order to prepare HITEC molten salt mixture, the three different types of salt nitrate/nitrite, KNO_3 and NaNO_3 were purchased from ACROS Organics with 99+% purity for analysis while NaNO_2 were purchased from Alfa Aesar with 97% purity. To enhance the thermophysical properties of HITEC salt, the following nanoparticles that were selected to be examined in combination with HITEC salt are aluminum oxide (Al_2O_3), titanium oxide (TiO_2), and multi-walled carbon nanotubes (MWCNT). Titanium dioxide and multi-walled carbon nanotubes integrated in HITEC molten salt has yet to be studied as current state of the art only focused on the mixture with solar salts. Aluminum oxide and titanium oxide were procured from Alfa Aesar while the multi-walled carbon nanotubes were procured from Graphene Supermarket. The size, thermal conductivity (K) and purity of the selected nanoparticles are tabulated in table 1 as provided by respective vendor and literature review. Additionally, four different wt.% composition of nanoparticles that were selected to be doped with HITEC are: 0.06%, 0.1%, 0.5% and 1%.

Different methods of preparing molten salt mixtures have been reported over the years [17, 24, 53]. In this study, HITEC salt was prepared by following the liquid dispersion method in order to achieve a reliable and uniform mixture. First, a batch of HITEC salt was prepared using the weight composition of 53% KNO_3 , 40% NaNO_2 and 7% NaNO_3 that was measured using a Mettler Toledo balance and placed inside a graduated

Table 1: Properties of Selected Nanoparticles [26, 60]

Nanoparticle Name	Size (nm)	K (W/m ² K)	Purity (%)
Al ₂ O ₃	40-50	6.2-10.9	99.5
TiO ₂	15	7.4-10.4	99.7
MWCNT	50-85	up to ~ 3000	>94.0

cylinder. Following that, approximately 250mL of deionized water was added into the graduated cylinder and the salts are allowed to dissolve in the deionized water, making a HITEC solution. The solution was then allowed to sit in ambient room temperature until all the solid salt particles are completely dissolved. More deionized water was added periodically to help with the dissolving process of the salts and the total volume of the final mixture was at 300mL. Based on mass of the selected nanoparticles percentages for an approximate total sample mass of 8g and using the concentration of HITEC solution (mg HITEC/mL solution), the volumes of solution required for each of the 13 samples were calculated and added to each respective vial. Subsequently, a total of 13 vials consisting of pure HITEC and HITEC + nanoparticles were prepared. All 13 vials were then placed in a Branson 1800 ultrasonicator bath for approximately 200 minutes at 69°C to obtain a homogeneous mixture between the base HITEC salt with nanoparticles. After sonication, all the vials were placed in an oven at 130°C for approximately 7 hours and at 115°C for an additional 2 hours to dry the samples without melting the HITEC salt. Prior to preparing and TGA or DSC samples of the HITEC salt, the salt mixture will first be set in the

oven at approximately 115°C to be dried for at least 30 minutes as drying of the HITEC salts is an important step due to nitrate salts hygroscopic behaviour when exposed to the atmosphere [28, 54].

While HITEC salts have been reported to have thermal stability up until 535°C [62], a TGA test was still conducted to verify that the HITEC sample prepared holds the same characteristic as reported by other researchers. The HITEC salt was tested in the range of 0°C to 600°C and the results shows that the prepared HITEC salt only experiences decomposition of ~1 wt.% in the specified temperature range.

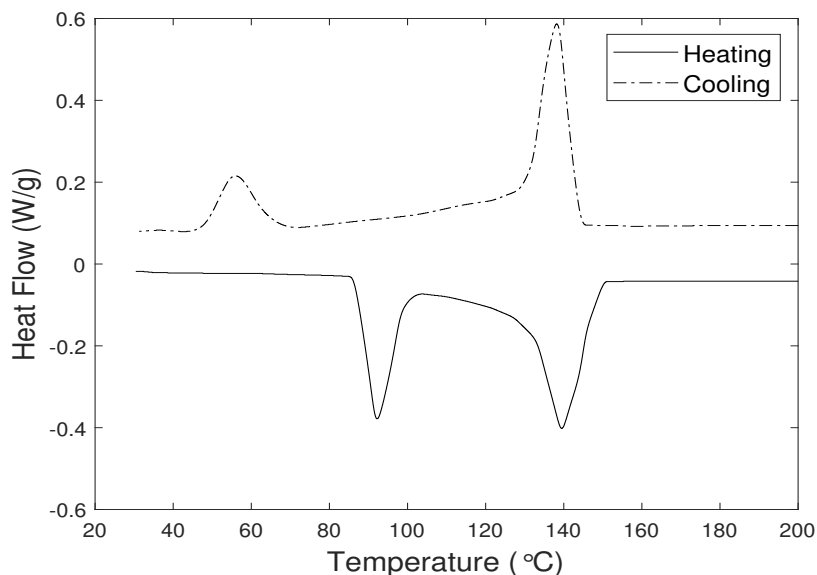


Figure 2: Heat Flow versus Time of Pure HITEC Salt (Averaged across three samples)

On the DSC test, all 13 samples of HITEC and HITEC + nanoparticles were tested in a heating/cooling range of 25°C to 200°C. Figure 2 depicts the thermophysical properties from the DSC test of the pure HITEC salt. The double peaks in the heating curve in figure 2 is due to the nature of the material itself where the first peak represents the loss

of water before it undergoes a solid-liquid phase change in the second peak [17]. Table 2 tabulates the DSC results averaged across 3 samples tested.

Table 2: Thermophysical Properties of Pure HITEC and HITEC + Nanoparticles

Material	T_m Onset (°C)	T_m Peak (°C)	T_f Onset (°C)	H (kJ/kg)	c_{pl} (J/g°C)
Pure HITEC	116.76	131.42	135.60	225.17	1.465
HITEC + 0.06% TiO ₂	115.45	129.95	135.10	175.54	1.195
HITEC + 0.1% TiO ₂	115.61	128.98	136.11	199.59	1.171
HITEC + 0.5% TiO ₂	128.46	138.24	139.94	158.93	1.025
HITEC + 1% TiO ₂	128.13	138.65	144.67	178.21	1.086
HITEC + 0.06% Al ₂ O ₃	126.76	138.57	139.87	244.76	1.346
HITEC + 0.1% Al ₂ O ₃	136.16	144.25	142.54	140.72	1.198
HITEC + 0.5% Al ₂ O ₃	122.11	133.97	132.97	219.09	1.239
HITEC + 1% Al ₂ O ₃	124.51	137.54	133.93	191.77	1.315
HITEC + 0.06% MWCNT	135.60	144.10	146.80	137.7	1.159
HITEC + 0.1% MWCNT	127.4	138.40	142.20	168.3	0.934
HITEC + 0.5% MWCNT	122.3	134.60	141.2	166.9	1.056
HITEC + 1% MWCNT	135.4	143.90	146.50	150.80	0.755

From Table 2, it can be seen that even with the addition of nanoparticles, there is no significant improvement in thermophysical properties of the HITEC mixture particularly when analyzing the specific heat capacity characteristics. Besides, the still rather high melting temperature of the HITEC salt was deemed unsuitable for a system with moderate operating temperature of 150°C. A substantial amount of energy will be required to power

the booster/backup system to melt the salt completely before it can be activated and flow through the entire system – which consequently increases the overall cost of operation. Hence, a different alternative for HTF that has a lower melting temperature as well as high specific heat capacity was investigated in the following section.

2.3 Erythritol as HTF

In order to match the operating temperature of approximately 150°C, a PCM with lower melting temperature than the HITEC salt will be required. Hence, erythritol which reportedly has the melting temperature of 118°C was selected to be studied. The pure erythritol used in this study was purchased from BulkSupplements.com. A small sample of approximately 10mg of erythritol was first tested in the TGA using the temperature range of 0-300°C. It was found that the erythritol starts decomposing approximately at 180 °C. Based on the TGA test, a temperature range of -25°C-170°C was defined for the following DSC test.

Figure 3 shows results of the melting and crystallization phenomena of erythritol in a heating/cooling cycle in the DSC. The sub-cooling effect of erythritol can be seen where the melting onset (T_m Onset) begins at approximately 110.34°C while the freezing onset (T_f Onset) starts at approximately 79.46°C. The melting onset and freezing onset difference of roughly 30°C makes erythritol a strong candidate as an HTF due to erythritol's ability to stay in liquid form for a longer period of time to prevent thermal expansion from crystallizing as well as transferring heat for a longer period of time. For thermal

energy storage applications, this sub-cooling behavior of erythritol is often deemed a disadvantage as it starts releasing the stored heat in the form of latent heat only when it cools down to a very low temperature (solidification initiation). However, it is this particular sub-cooling characteristic of erythritol that makes it desirable as a HTF. Besides, thermal expansion of erythritol during crystallization should be avoided at all cost as such reaction could ultimately yield to the breakage of copper tubes throughout the proposed system.

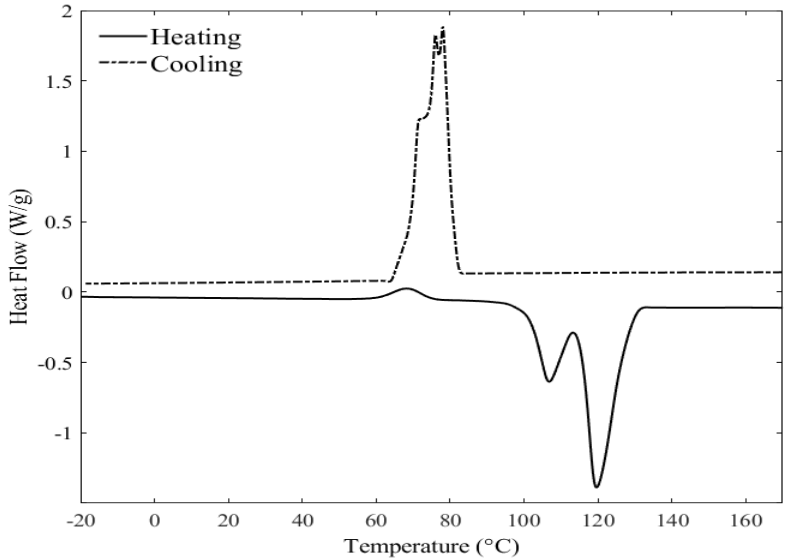


Figure 3: Heat Flow versus Time of Erythritol (Averaged across three samples)

2.4 Erythritol + 1% MWCNT + TEA as HTF

To further improve the heat transfer properties of pure erythritol, MWCNTs were added with triethanolamine (TEA) as a dispersant to aid with a homogeneous and uniform mixture between the erythritol and MWCNT. Two individual vials were prepared

Table 3: Thermophysical Properties of Pure Erythritol

T_m Onset ($^{\circ}\text{C}$)	110.34
T_m Peak ($^{\circ}\text{C}$)	114.81
T_f Onset ($^{\circ}\text{C}$)	79.46
T_f Peak ($^{\circ}\text{C}$)	76.09
c_{pl} ($\text{J/g}^{\circ}\text{C}$)	2.59
H (kJ/kg)	291.57

for molten Erythritol samples with one vial to be doped with MWCNT at a concentrations of 1.0 wt.% and a second vial doped with 1 wt.% MWCNT and an added 0.5 wt.% TEA dispersant. Molten erythritol was added to each vial for an approximate mass of mixture at the specified concentrations. All sealed vials were then placed in a sonicator at its maximum temperature 69°C for 200 minutes to thoroughly disperse nanoparticles throughout the mixture. Following the sonicator, all sample vials were placed in a 115°C oven with caps removed for approximately 2 hours to remove any water from the mixture. Fully dried samples were allowed to cool to room temperature in the closed oven, then capped and placed in a desiccator for storage while awaiting testing in TGA and DSC. A small sample of approximately 10mg for each mixture was tested in TGA and all mixtures showed to be stable below 200°C and were approved for testing in DSC at the -25 - 180°C range.

Table 4 compares the DSC results of erythritol + MWCNT + TEA results with the pure erythritol results from the preceding section. It can be seen that with the addition of

TEA in Mixture 2 yields to an increase in specific heat capacity of approximately 12.4% when compared to the pure erythritol sample. Besides, there is also a decrease in freezing onset temperature (sub-cooling) of approximately 5°C. This is an important achievement as the prolonged sub-cooling effect allows for erythritol to maintain in liquid form for a longer period of time inside the U-tubes. This proves that with the addition of TEA a more uniform mixture between erythritol and MWCNT can be achieved.

Table 4: Erythritol Melting/freezing and Specific Heat Capacity Comparison

Material	Erythritol	Mixture 1	Mixture 2
T_m Onset (°C)	110.34	114.82	114.41
T_m Peak (°C)	114.81	118.83	118.68
T_f Onset (°C)	79.46	78.81	74.81
$C_{p,l}$ (J/g°C)	2.585	2.381	2.905
H (kJ/kg)	291.6	304.7	328.9
Mixture 1: Erythritol plus 1% MWCNT			
Mixture 2: Erythritol plus 1% MWCNT, 0.5% TEA			

2.5 Comparison of HITEC Salt and Erythritol as HTF

When comparing the DSC test results between pure HITEC salt, HITEC salt + nanoparticles, and erythritol, it was determined that erythritol would make a better HTF as a PCM for the dual-PCM EUTC system due to the following reasons:

1. Sub-cooling behaviour of erythritol in the cooling curve which allows erythritol

to maintain in liquid form for an extended time. This is a particularly important property when utilizing the latent heat release in erythritol.

2. Erythritol has a lower melting temperature. This makes erythritol a better match in combination with PCM72. Besides, lesser energy in the booster/backup will be required to melt the erythritol completely before initiating the system.
3. Pure erythritol has a higher specific heat capacity value than pure HITEC and HITEC + Nanoparticles.
4. Pure erythritol has a higher latent heat of fusion than pure HITEC and HITEC + Nanoparticles.
5. The addition of MWCNT nanoparticles with a small amount of TEA dispersant further increases the specific heat capacity and thermal conductivity of erythritol [21], yielding to a higher rate of heat transfer as a HTF. It was also observed that there is an enhancement in latent heat of fusion of erythritol with the addition of MWCNT nanoparticles.

Based on the reasons stated above, pure erythritol and erythritol + MWCNT + TEA was selected to be analyzed as the HTF integrated in the dual-PCM EUTC in the following chapter.

CHAPTER 3

DESIGN AND MODELING OF AN EVACUATED U-TUBE COLLECTOR INTEGRATED WITH DUAL-PCM CONFIGURATION

For this work, a CFD modeling of the proposed system has been investigated using ANSYS Fluent R19.2 software.

3.1 System Configuration

Figure 4 shows the configuration of the proposed system. The ETC is integrated with Tritriacontane paraffin (PCM72) with the melting point of 72°C, while the U-tube is filled with the selected HTF. The selected HTF will be stored in the HTF storage tank with a backup booster system incorporated to heat the HTF up during times where no sun is available. During the day, HTF will be heated and energy will be stored as it passes through the ETC. It will then be pumped into the water storage tank which serves as a heat exchanger where the HTF effectively provides hot water for various household or commercial activities such as heating, ventilating, and air conditioning systems. As the HTF releases heat to the water storage tank, it cools down and passes back into the HTF storage tank and the cycle continues.

Simulation modeling of a transient model of U-tube integrated ETC system is performed in stagnation (on-demand) operation. The CFD analysis of the proposed system is initiated by considering both PCM and erythritol to be fully melted at the temperature of $\sim 150^{\circ}\text{C}$. It is assumed that there will be no more solar radiation during the operation of

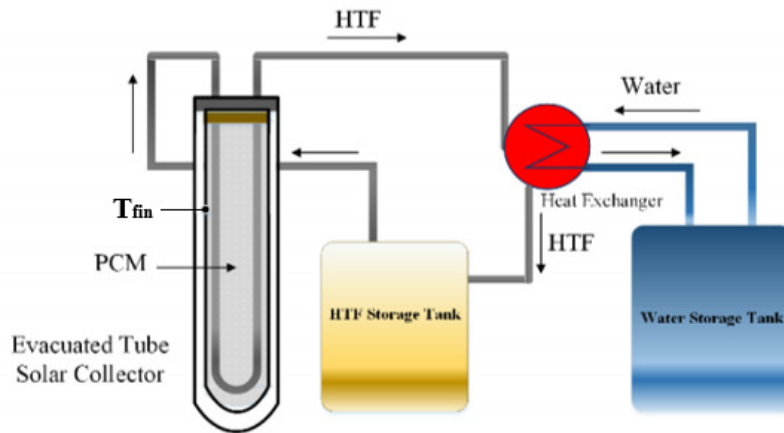


Figure 4: Schematic of the dual-PCM EUTC SWH System

the system. Therefore, natural convection between PCM and water in the heat exchanger was defined for the cooling process of the system.

3.2 Computational Fluid Dynamics Modeling

3.2.1 ANSYS Geometry

The ETC consists of two concentric glass tubes with the vacuum layer in between that prevents heat loss through convection. In this paper, the 3D model of a single U-Tube integrated ETC is used in this simulation with PCM72 filling the PCM region and several different types of HTF filling the U-tube. Such configuration effectively replaces the heat pipe in commercially available ETCs. The specifications of the U-tube ETC such as dimensions and properties of glass tube, U-tube and fin are listed in Table 5. Table 6 also shows the thermophysical properties of the selected PCM and HTFs. These specifications from Table 5 and Table 6 were defined as boundary conditions in FLUENT. During the day when the tube is exposed to sunlight, solar energy is absorbed by the solar selective

coating which effectively heats up HTF ready for use in the U-tube.

The 3D geometry of the model was first constructed on ANSYS design modeler as seen in figure 5. The outertube and innertube is defined as a transparent borosilicate glass. Meanwhile, the aluminum fin is then considered as part of a conduction layer defined in FLUENT with a thickness of 0.2mm. The U-tube is then defined as a copper tubing with wall thickness of 0.1mm. A simple condenser section (Figure 6a) was also constructed by extending one side of the U-tube geometry where in this condenser section the HTF in the U-tube heats transfers heat to heat water up as if in a simple heat exchanger configuration. The complete dimensions and specifications of the U-tube integrated ETC are tabulated in table 5. Besides, the thermophysical parameters of the selected material used as PCM and HTF in Fluent can be found in table 6 and 7.

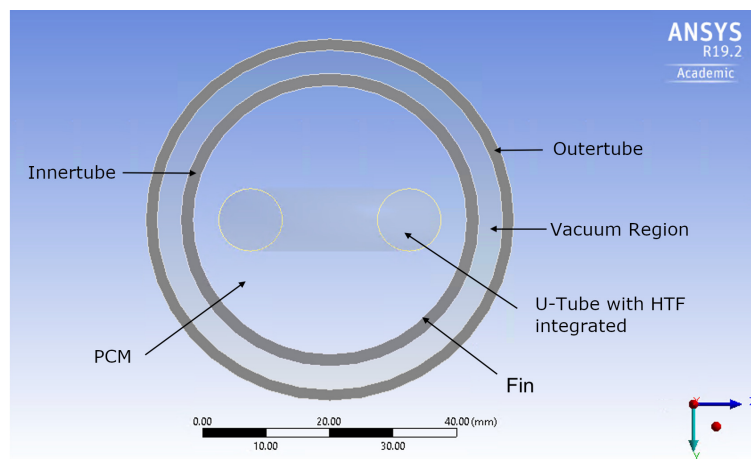


Figure 5: U-Tube ETC Geometry

Table 5: Specification of U-Tube Integrated ETC [15, 39, 41].

Component	Properties	
Glass Tube (Borosilicate)	Density (kg/m^3)	2230
	Specific heat (J/kg-K)	980
	Thermal conductivity (W/m-k)	1.14
	Outer tube diameter (m)	0.058
	Inner tube diameter (m)	0.047
	Thickness (m)	0.0018
	Length (m)	0.5
U-Tube (Copper)	Density (kg/m^3)	8978
	Specific heat (J/kg-K)	381
	Thermal conductivity (W/m-k)	387.6
	Tube diameter (m)	0.008
	Thickness (m)	0.0001
Fin (Aluminum)	Density (kg/m^3)	2719
	Specific heat (J/kg-K)	871
	Thermal conductivity (W/m-k)	202.4
	Outer diameter (m)	0.0358
	Thickness (m)	0.0002

3.2.2 Meshing

Generating a suitable mesh for any CFD simulation is important as meshing affects the quality, speed, and accuracy of the simulation. Figures 7 and 6 illustrates the mesh generated for this geometry from different views.

To achieve uniform mesh in Fluent meshing, the ETC geometry is divided into 4 different parts and applying a combination of hexahedral and tetrahedral meshes (Figures

Table 6: Thermophysical Properties Latent Heat Storage PCM72 [34]

PCM	Melting temperature (K)	345
(Tritriacontane)	Density (liquid) (kg/m^3)	782
($C_{33}H_{68}$)	Density (solid) (kg/m^3)	810
	Specific heat (liquid) (kJ/kg-K)	1.11
	Specific heat (solid) (kJ/kg-K)	0.87
	Thermal conductivity (W/m-k)	0.21
	Latent heat of fusion (kJ/kg)	256
	Viscosity (kg/m-s)	0.026
	Thermal Expansion Coefficient (1/K)	0.000154
	Solidus temperature (K)	338.83
	Liquidus temperature (K)	347.18

7a and 7b). In addition, the U-tube geometry is further divided as a butterfly-grid, or also known as orthogonal-grid (O-grid) mesh using hexahedral meshes as shown in Figure 7c. Butterfly-grid style meshes are often desirable when analyzing a flow with heat transfer problem in a cylindrical pipe as it allows for users to have better control over the mesh quality as well as yielding to the best distribution of mesh [23]. Inflation layers around the walls of the U-tube was applied to ensure that the melting and solidification behaviour of material closer around the U-tube walls can be captured. For the PCM region, tetrahedral meshes were used by applying body sizing with element sizes of 0.002m. A total of 416,398 number of nodes were generated for this model. To ensure sufficient quality of the mesh generated, mesh skewness and mesh orthogonal quality was monitored where the minimum orthogonal quality was kept to be >0.1 and the maximum skewness was maintained <0.9 .

Table 7: Thermophysical Properties of Selected HTF [21, 25, 29, 40, 48]

Erythritol ($C_4H_{10}O_4$)	Density (liquid) (kg/m^3)	1300
	Specific heat (liquid)(kJ/kg-K)	2.585
	Thermal conductivity (W/m-k)	0.326
	Viscosity (kg/m-s)	0.01602
Ethylene-Glycol ($C_2H_6O_2$)	Density (liquid) (kg/m^3)	1111.4
	Specific heat (liquid)(kJ/kg-K)	2.415
	Thermal conductivity (W/m-k)	0.252
	Viscosity (kg/m-s)	0.0157
Silicone Oil	Density (liquid) (kg/m^3)	832
	Specific heat (liquid)(kJ/kg-K)	1.515
	Thermal conductivity (W/m-k)	0.133
	Viscosity (kg/m-s)	0.0175
Erythritol + 1% MWCNT + TEA	Density (liquid) (kg/m^3)	1300
	Specific heat (liquid)(kJ/kg-K)	2.905
	Thermal conductivity (W/m-k)	0.55
	Viscosity (kg/m-s)	0.0189

3.2.3 Boundary Conditions

ANSYS Fluent solves the conservation of equations for mass and momentum for all flows. Energy conservation was also solved in this case as this is a heat transfer simulation. Moreover, melting/solidification model was used to portray the melting/solidification behavior of the PCM. To simplify the model, several assumptions were made following the simulation:

- No heat loss or gain from the surrounding;

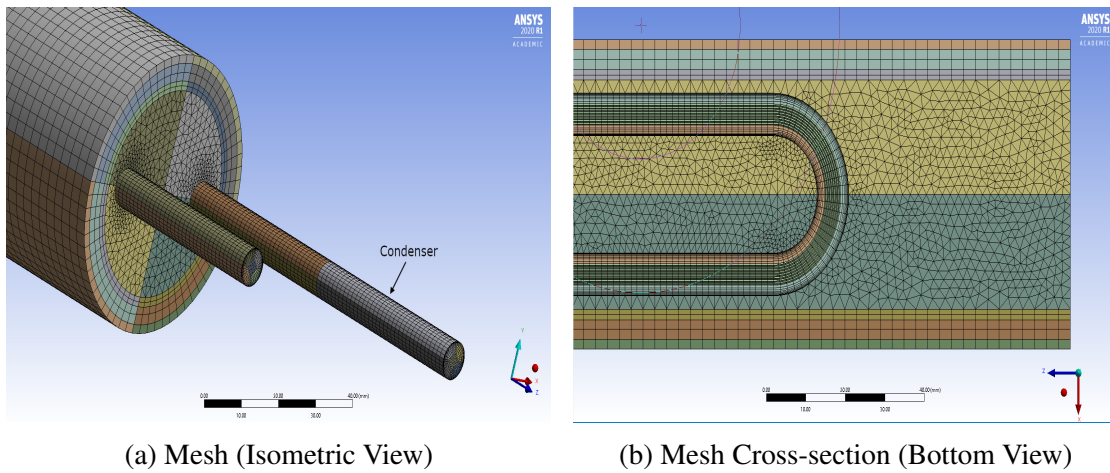


Figure 6: Meshing from Isometric and Cross-section View of U-Tube ETC

- Flow in the U-tube is laminar and incompressible. Reynolds number or erythritol was calculated to be less than 2300 using the relation from equation 3.1:

$$Re = \frac{\rho v d}{\nu} \quad (3.1)$$

where,

ρ is density;

v is the velocity = mass flow rate/ ($\rho \times \pi \times 0.004^2$)m/s;

d = diameter of U-tube = 0.008m;

ν = viscosity

Finally, Reynolds Number was found to be $Re = 125.2$ for erythritol, $Re = 127.7$ for ethylene-glycol, $Re = 114.6$ for silicone oil, and $Re = 106.1$ for erythritol + MWCNT, validating that flow for all the materials is laminar.

- Constant thermophysical properties of PCM;

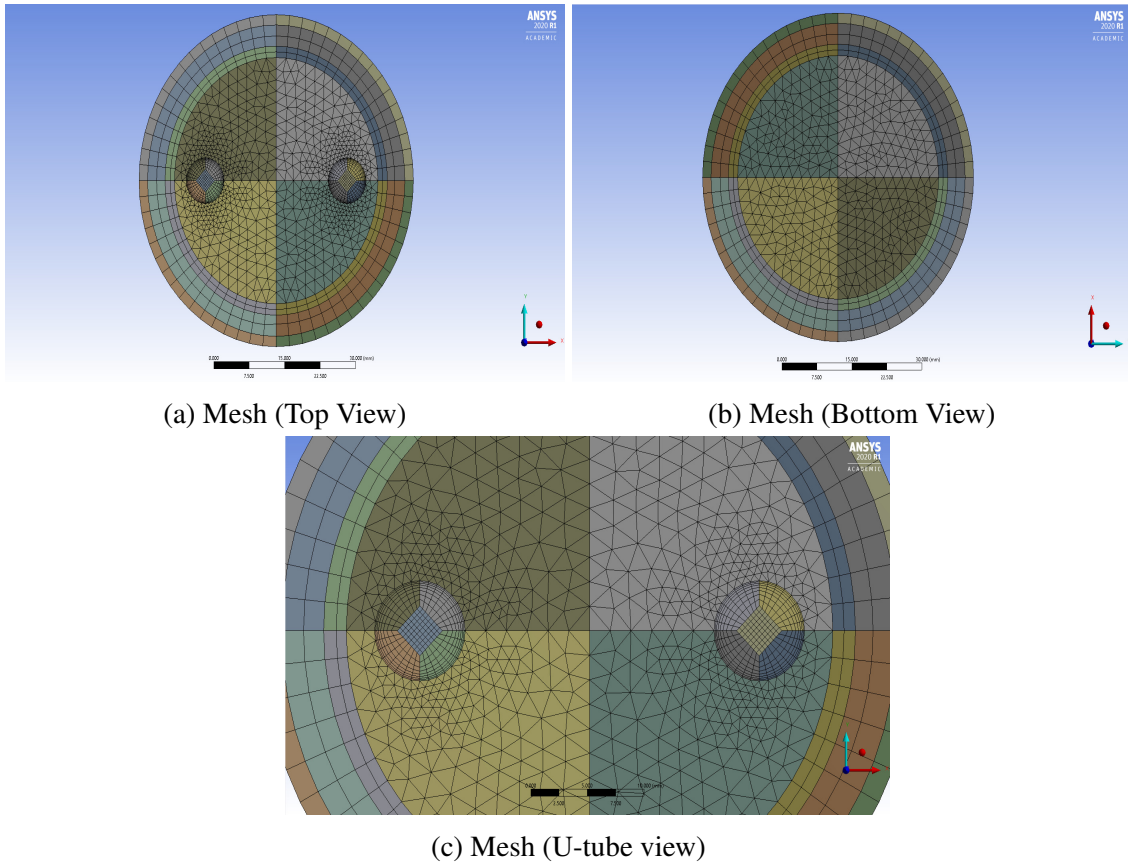


Figure 7: Meshing from Top and Bottom View of U-Tube ETC

- Boussinesq approximations are assumed to be valid for density variation of PCM to aid in faster convergence for natural convection flows [15, 41]. This assumption is valid when:

$$\beta(T - T_{mean}) \ll 1 \quad (3.2)$$

where,

β is the thermal expansion coefficient of the material and;

$$T_{mean} = (T_{solidus} - T_{liquidus})/2$$

For boundary conditions, a mounting angle of 45° was implemented as recommended by manufacturer as well as to match with the mounting angle used from previous experimental setup [5, 39]. For the condenser section, natural convection of water was applied by defining the heat transfer coefficient of water at $500\text{W/m}^2\text{K}$. A mass flow rate of 0.0126kg/s was also used when defining the inlet flow rate of the U-tube. Furthermore, a user defined function (UDF) was also created to record and store average temperature at the surface of the outlet of the U-tube [19]. This UDF code records temperature at the surface of the outlet of the U-tube to be used as the inlet temperature of the U-tube for the following iteration, creating a closed loop piping system. Figure 8 shows the temperature profile UDF code interpreted in Fluent.

The vacuum region was defined such as having properties of air but with very low thermal conductivity and very low specific heat capacity to prevent any heat transfer through conduction [14, 41]. Temperature of vacuum is also set as a fixed value of 298K throughout the simulation in Fluent. Material and boundary conditions specifications defined in Fluent for this study can be found from table 5 and 6. Moreover, thermophysical properties of ethylene-glycol used can also be found pre-defined in Fluent's fluid database.

3.2.4 Governing equations

Governing equations of continuity, momentum, and energy equations were simultaneously solved and the continuity equation is defined in Fluent [18]. The continuity equation is defined as:

$$\frac{\partial \rho}{\partial t} + \nabla(\rho \vec{v}) = 0 \quad (3.3)$$

```

1 #include "udf.h"
2 #include "mem.h"
3 #include "prf.h"
4 #include "para.h"
5
6 real Tavp; /* defined outside because will be used in multiple DEFINE macros */
7
8 DEFINE_EXIT(outlet_temp)
9 {
10 /* Variables used by host */
11
12 int surface_thread_id=0;
13 real total_area=0.0;
14 real total_temp=0.0;
15 /* real Tavp=0.0; */
16
17 /* "Parallelized" Sections */
18 /* Compile this section for computing processes only(these variables are not available on the host) */
19
20 #if !RP_HOST
21 Domain *domain = Get_Domain(1);
22 Thread *thread;
23 face_t face;
24 real area[ND_DIM];
25 #endif
26
27 /* Sending data from host to node */
28 host_to_node_int_1(surface_thread_id);
29
30 /* Summing code on host, to calculate face area and temperature */
31 #if !RP_HOST
32
33 /* thread is only used on compute processes */
34 thread = Lookup_Thread(domain,surface_thread_id);
35 begin_f_loop(face,thread)
36
37 /* If this is the node to which face "officially" belongs,*/
38 /* the total area and total temp values for this node */
39
40 if (PRINCIPAL_FACE_P(face,thread))
41 {
42 F_AREA(area,face,thread);
43 total_area += NV_MAG(area);
44 total_temp += NV_MAG(area)*F_T(face,thread);
45 }
46 end_f_loop(face,thread)
47
48 /* Perform node synchronized actions */
49 #if RP_MODE
50 total_area = PRF_GRSUM1(total_area);
51 total_temp = PRF_GRSUM1(total_temp);
52 Tavp = (total_temp/total_area);
53 #endif /* RP_MODE */
54
55 #endif /* !RP_HOST */
56
57 /* Pass the node's total area and temperature to the Host for averaging */
58
59 node_to_host_real_3(total_area,total_temp,Tavp);
60
61 /* Collecting the temperature values from nodes and printing out the values on console */
62 #if RP_MODE
63 /* Message("Total Area After Summing: %f (m2)\n",total_area); */
64 /* Message("Total temp After Summing %f (K)\n",total_temp); */
65 Message("Average temperature on Surface %d is %f (K)\n",surface_thread_id,Tavp);
66 #endif /* !RP_MODE */
67 }
68
69 DEFINE_PROFILE(inlet_temp,t,i)
70 {
71 face_t f;
72 /* "Parallelized" Sections */
73 /* Compile this section for computing processes only, variables are not available on the host */
74
75 begin_f_loop(f,t)
76 {
77 F_PROFILE(f,t,i) = Tavp;
78 }
79 end_f_loop(f,t)
80
81 Message("Average temperature at inlet %f (K)\n",Tavp);
82
83 }

```

(a) UDF Code

(b) UDF Code (continued)

Figure 8: User Defined Functions (Temperature Profile)

where ρ and \vec{v} denotes the density and velocity vector.

Meanwhile, momentum equation is defined as:

$$\frac{\partial}{\partial t}(\rho\vec{v}) + \nabla(\rho\vec{v}\vec{v}) = -\nabla p + \nabla\vec{\tau} + \rho\vec{g} + S_g \quad (3.4)$$

Where p denotes the pressure, τ is the stress tensor and g is the gravity acceleration.

Lastly, the energy equation for melting/solidification problems is written as below:

$$\frac{\partial}{\partial x}(\rho H) + \nabla(\vec{v}(\rho H + p)) = \nabla(k\nabla T + \vec{\tau}\vec{v}) + S_H \quad (3.5)$$

Where H is the internal energy, sum of sensible enthalpy h and latent heat ΔH of the

PCM, and k is the thermal conductivity. The sensible enthalpy h can be found as below:

$$h = h_{ref} + \int_{T_{ref}}^T c_p dT \quad (3.6)$$

In which h_{ref} and T_{ref} is the reference enthalpy and reference temperature, and c_p is the specific heat at constant pressure. Meanwhile, latent heat ΔH is calculated using the equation below:

$$\Delta H = \beta L \quad (3.7)$$

Where β is the liquid fraction of the PCM and L is the latent heat of PCM. The liquid fraction β is then further defined by Fluent as:

$$\begin{aligned} \beta &= 0, \quad \text{if } T < T_{solidus} \\ \beta &= 1, \quad \text{if } T > T_{liquidus} \\ \beta &= \frac{T - T_{solidus}}{T_{liquidus} - T_{solidus}}, \quad \text{if } T_{solidus} < T < T_{liquidus} \end{aligned} \quad (3.8)$$

Furthermore, the stress tensor $\vec{\tau}$ equation is as follow:

$$\vec{\tau} = \mu[(\nabla\vec{v} + \nabla\vec{v}^T) - \frac{2}{3}\nabla \cdot \vec{v}I] \quad (3.9)$$

In which μ is molecular viscosity and I is the unit tensor. Finally, for natural convection and mushy region, the source term S_g was considered as follow [41]:

$$S_g = \rho\vec{g}\beta(T - T_{ref}) - \frac{(1 - \beta)^2}{\beta^3 + \epsilon} A_{mushy}\vec{v} \quad (3.10)$$

The second term in equation 3.10 relates to the porosity of porous medium in each cell where liquid fraction is considered [41]. A_{mushy} is the mushy zone constant which was set at 100000. Meanwhile, to avoid a division by zero, ϵ was set as a very small number of 0.001 [18].

In the FLUENT solver, a pressure-based solver was utilized and the SIMPLE algorithm scheme with PRESTO! mode was used. Least square cell based was used to solve for gradient with Second Order Upwind mode used to solve for Momentum and Energy. Meanwhile, convergence criteria of 10^{-6} was selected for continuity and momentum while a convergent criteria of 10^{-8} for energy equations. For solution control methods, pressure, momentum and liquid fraction were under-relaxed by factors of 0.3, 0.5 and 0.9 respectively in order to achieve stable convergence. The simulation was simulated for 3 hours using time step size between 0.1s and 1s based on convergence.

CHAPTER 4

CFD RESULTS AND DISCUSSION

For this study, CFD simulation of the system in stagnation (on-demand) operation was investigated. Stagnation operation can be defined such as there is no circulation of HTF throughout the system as the ETC absorbs solar radiation during the day, allowing the ETCs to achieve maximum energy storage that can be used when circulation of HTF is initiated in the system at a later time of the day [39]. Stagnation operation only has approximately 3 hours worth of simulation data while the normal operation (where HTF circulates the system all day) has 24 hours worth of simulation data. As this is a completely new system that is being studied with no prior experimental work or data, preliminary analysis in stagnation operation effectively reduces overall computational time.

4.1 Comparison of Heat Pipe ETC and Dual-PCM EUTC Performance

Figure 9 depicts the fin temperature over 140 minutes of stagnation operation of the proposed dual-PCM EUTC, with pure erythritol as a HTF, in comparison with the obtained results for HPETC integrated with PCM72 from previous experimental work [39]. In the experimental analysis, the system was set outside without any cooling throughout the day, once the fin temperature reaches to approximately 150°C, the cooling was initiated. To cross-validate the experimental results, the CFD modeling of the dual-PCM EUTC was initialized at 150°C. From figure 9, it can be observed that the flat-lining of

fin temperature in both systems begins at approximately 25 minutes of data collection. This is due to the latent heat release from PCM72 once the temperature in the tube is below the solidus temperature. As PCM72 solidifies, latent heat is being released into the tube collectors, hence keeping the fin at a rather constant temperature. The solidification phenomena of PCM72 can be seen from figure 10 which depicts the liquid fraction of PCM72 over time. PCM72 is fully melted at liquid fraction of 1 and is fully solidified at liquid fraction of 0. After 120 minutes, as it can be seen in both figure 9 and 10, PCM72 is solidified completely, hence the fin temperature once again experiences a steeper drop as there is no more latent heat being released into the system.

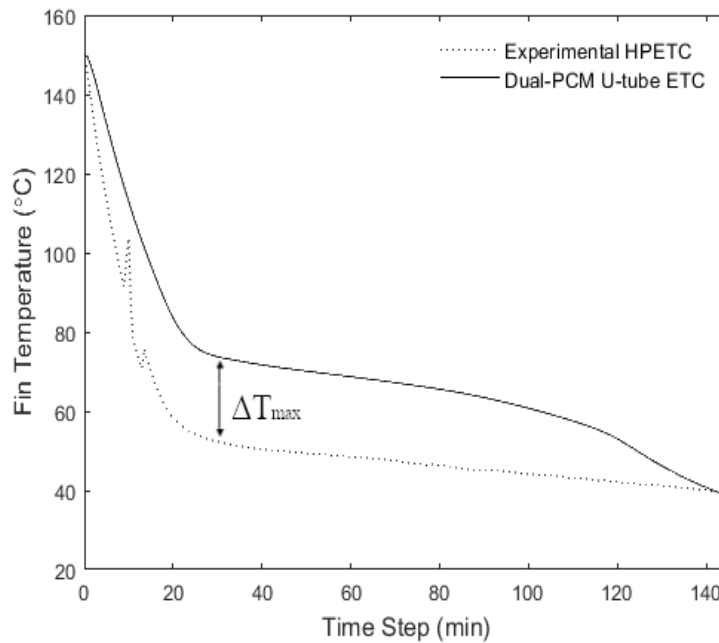


Figure 9: Fin Temperature Inside ETC versus Time

As it can be seen in figure 9, the dual-PCM EUTC exhibits enhanced performance as it maintains a higher fin temperature of the tube collector than the traditional HPETC

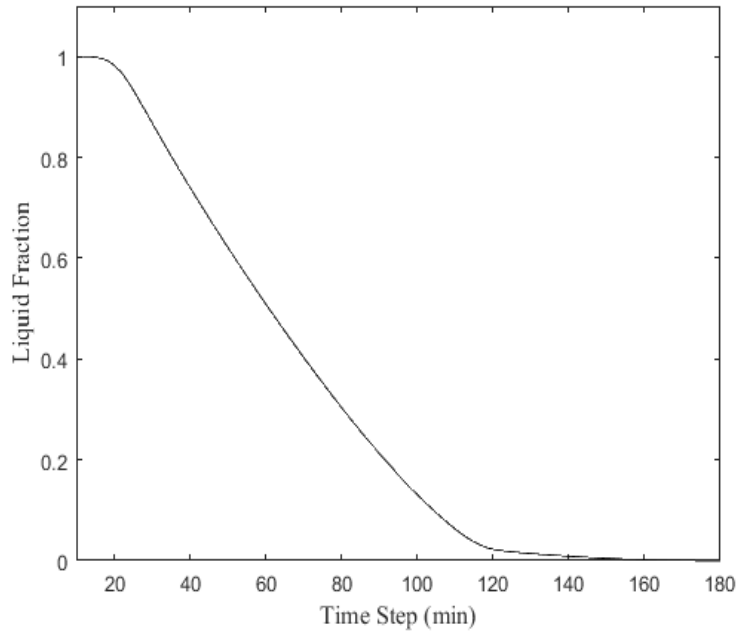


Figure 10: Liquid Fraction of PCM72 Inside ETC versus Time

system at a max temperature difference (ΔT_{\max}) of approximately 24°C . This enhancement is due to the heat pipe vs U-tube characterization. The HPETC system has only a single droplet of HTF in the copper heat pipe, therefore, the heat is absorbed by conduction through the copper surface and then is transferred by free convection to the water in the manifold at the bulb of the heat pipe. Conversely, the dual-PCM EUTC demonstrates a higher amount of sensible heat inside the tube due to the high specific heat capacity as well as large amount of the selected HTF. This results in larger heat extraction from the tube, therefore, faster initiation of solidification process of PCM72. Consequently, the large amount of stored heat will be released back to the tube, keeping the fin temperature at a higher value compared with the HPETC.

Sensible heat and latent heat transfer in the tube collectors can be calculated using equations 4.1 and 4.2 below:

$$\dot{q}_{sensible} = \dot{m}C_p\Delta T \quad (4.1)$$

$$q_{latent} = mH \quad (4.2)$$

where q is the energy, \dot{q} is the power, m is the mass of the PCM, \dot{m} is the mass flow rate of the HTF in the U-tube, C_p is the specific heat capacity, H is the latent heat of fusion, and ΔT is the difference in temperature between the outlet temperature before erythritol enters the condenser section and inlet temperature of the U-tube. In the dual-PCM EUTC system, the mass of PCM72 filled in the tube collectors was calculated to be approximately 0.5kg based on PCM72's density and volume of the inner tube collector. The latent heat of the dual-PCM EUTC system can then be calculated as follow:

$$q_{latent} = (mH)_{PCM} = (0.5kg)(256kJ/kg) = 128kJ \quad (4.3)$$

In addition to latent heat energy from the PCM72 which acts as a backup heat, the dual-PCM EUTC system has a significant amount of sensible heat energy from the erythritol flowing through the U-tube inside the tube collectors. At the time when ΔT_{max} between both system occurs, the rate of sensible heat can be calculated as follow:

$$\dot{q}_{sensible} = \dot{m}C_p\Delta T = (0.0126kg/s)(2.585kJ/kgK)(327.77 - 325.98)K = 0.06kW \quad (4.4)$$

At approximately 30 minutes from figure 9 where the ΔT_{max} occurs, the maximum sensible heat transfer is 0.06kW as calculated from equation 4.4.

4.2 Comparison of Different HTF in dual-PCM EUTC

From the previous section, it can be deduced that the dual-PCM EUTC system showed improved performance when compared to the commercially available HPETCs in terms of a higher fin temperature. In this section, the effect of heat transfer on the U-tube ETC system using silicone oil, ethylene-glycol, erythritol, and erythritol + MWCNT + TEA as HTF was investigated. Where silicone oil and ethylene-glycol are commonly used HTFs in commercial systems, the use of erythritol and erythritol + MWCNT + TEA has never been studied before. Identical with the previous section, PCM72 was also integrated in the tube collector for latent heat storage here. Figure 11 below shows the CFD results of fin temperature by using different types of HTF with 3 hours of simulation time.

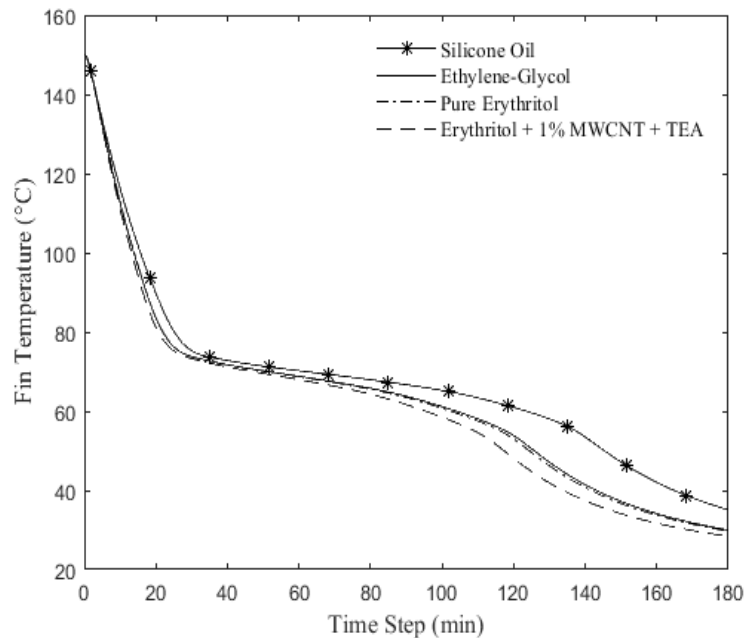


Figure 11: Fin Temperature Using Different HTF Inside ETC versus Time

Based on figure 11, silicone oil, which has poorest heat transfer properties compared to the other selected HTFs, showed a significantly higher fin temperature during the stagnation operation while the HTF that has the more superior heat transfer properties such as the erythritol + 1% of MWCNT showed the lowest fin temperature. In the U-tube ETC system, the higher the heat transfer rate, the more heat is being extracted to the water on the condenser section. It can be predicted that by using HTFs with enhanced thermo-physical properties in this system configuration will release more heat at the condenser to provide more hot water to the demand side. This consequently lowers the fin temperature in the tube collector. Based on this figure, it can be deduced that by using materials with higher specific heat capacity and thermal conductivity as a HTF, the lower the overall fin temperature of the system.

For a HPETC with PCM filling the tube collectors, the higher the fin temperature in a stagnation operation the better the functionality of the system. As higher fin temperature in the HPETC configuration shows that there latent heat storage being released from the PCM into the heat pipe, providing hot water for an extended period of time during the time when there is no sun available. In the meantime for a dual-PCM EUTC system, which has a higher overall fin temperature compared to the HPETC system, the system's performance is deemed desirable when using a HTF that results in a lower fin temperature. The lower fin temperature is because the amount of heat transferred to the water cannot be balanced by the amount of heat provided by the PCM inside the tube collector – there is more heat being transferred to the demand side than there is the amount of heat

being released to the U-tube inside the ETC from the PCM in each loop, therefore resulting in lower fin temperature for HTFs that has higher specific heat capacity and thermal conductivity.

CHAPTER 5

CONCLUSION

In this study, a novel design of a solar water heating (SWH) system that combines the heat transfer and the phase change material (PCM) storage system both as a single unit is investigated. The selected type of collector for this purpose is an evacuated tube solar collector (ETC) and the new design, the dual-PCM EUTC, has been developed by applying a U-tube instead of heat pipe inside the ETC which contains the HTF. Besides, the use of PCM as a heat transfer fluid (HTF) to be integrated in this proposed dual-PCM EUTC system was also studied.

Firstly, thermal analysis of potential PCMs such as the HITEC molten salt and erythritol was carried out using the Thermogravimetric Analyzer (TGA) and Differential Scanning Calorimeter (DSC) to study their thermal properties and behaviour through the process of heating and cooling. Nanoparticles such as aluminum oxide, titanium oxide, and multi-walled carbon-nanotubes (MWCNT) were used with the selected PCMs to further enhance the materials' thermophysical properties. The triethanolamine (TEA) dispersant was used in conjunction with MWCNT and erythritol to provide a more uniform mixture. Based on preliminary thermal analysis results, the HITEC molten salt was immediately ruled out due to its very high melting temperature and low specific heat capacity. Despite the addition of nanoparticles, HITEC salt would not be suitable for moderate operating temperature conditions of $\sim 150^{\circ}\text{C}$. Therefore, erythritol was chosen due to its

lower melting temperature and sub-cooling effect. When mixed with 1% of MWCNT nanoparticles and TEA, the freezing temperature (sub-cooling) of erythritol were lowered by approximately 5°C. As erythritol is prone to thermal expansion through the process of solidification, this is an important achievement as lowering the sub-cooling of the erythritol helps with maintaining the fluid characteristic of the erythritol inside the pipes of the solar water heating system. Furthermore, the specific heat capacity of samples with MWCNT and TEA showed a 12.4% enhancement when compared with pure erythritol. The exaggeration of sub-cooling behavior and increased specific heat capacity exhibited in the results of this study show promise for the use of this unique PCM-based HTF.

After determining erythritol as the most appropriate HTF, the proposed system configuration was then investigated using Computational Fluid Dynamic (CFD) modeling techniques to analyze the thermal behavior and for optimization of such configuration. The analysis has been done in stagnation (on-demand) operation. Parameters of HTF obtained from thermal analysis of HTF was then used as boundary conditions when setting up ANSYS Fluent. Moreover, the thermal performance comparison of the proposed dual-PCM EUTC vs the traditional heat pipe ETC has been done by comparing the averaged fin temperature inside the tube collector of each system. Both configurations have Tri-triacontane paraffin (PCM72) filled inside the tube collector as latent heat storage. The results from this CFD simulation shows a maximum of $\sim 24^{\circ}\text{C}$ increase in fin temperature of the of dual-PCM EUTC compared with the heat pipe ETC. This shows that the dual-PCM EUTC system will hold more heat inside the tube collectors for a longer period of time, subsequently providing more hot water for use during periods when there is no

sunlight available.

Further analysis using several different types of HTF was also investigated to determine its effects on the novel dual-PCM EUTC system. Commonly used HTF such as ethylene-glycol and silicone oil were selected to compare with the selected PCM-based HTF of pure erythritol and erythritol+MWCNT+TEA. Noticeably, using erythritol and erythritol+MWCNT+TEA as a HTF in the dual-PCM EUTC configuration leads to a lower fin temperature. This is due to the material's higher specific heat capacity and higher thermal conductivity when compared to the traditional HTFs. The phenomena of a lower fin temperature in conjunction with enhanced thermophysical properties of HTFs lead to the following prediction – the better the thermophysical properties of the HTF in the dual-PCM EUTC system, the more heat is being transferred from the circulating HTF to the condenser/demand side. Henceforth, leading to a lower overall fin temperature as more energy is being discharged from the tube collector to the demand side.

The results from this study can be applied to SWH in moderate operating temperature conditions. The proposed dual-PCM EUTC utilizing PCM-based HTF allows for an enhanced performance of the overall system's functionality during the period of time when little to no sunlight is available.

CHAPTER 6

FUTURE WORK

This study is part of a preliminary investigation to examine the effects of using PCM as a HTF for the proposed dual-PCM EUTC as well as utilizing CFD methods to further optimize and predict the behaviour of the system. Following this research, the dual-PCM EUTC will enter the experimental phase where the complete system configuration setup be put together at the new Renewable Energy roof platform. Conducting experimental work will help with a better understanding on the direct and indirect effects of this system where the system will be studied under both normal and stagnation (on-demand) operation. Moreover, future experimental work on the dual-PCM EUTC will also focus on monitoring the temperature of water in the water storage tank on the demand side to determine the overall efficiency of the system. It is important to note that as this dual-PCM EUTC design is novel, there is no actual experimental data or study available regarding this configuration yet. Future work will include cross validation and verification (V&V) of the current CFD model and simulation with fin temperature data that can be obtained from experimental work. This is a vital procedure as V&V of the current CFD model will further strengthen the overall confidence and reliability as well as assessing the accuracy of current CFD result. Another future work also includes optimizing thermophysical properties of erythritol as a PCM-based HTF to further improve the functionality and efficiency of the overall system.

APPENDIX A

INSTRUMENT PARAMETERS

Table A.1: TGA5500 Instrument Specification

Temperature Accuracy	$\pm 1^{\circ}\text{C}$
Temperature Precision	$\pm 0.1^{\circ}\text{C}$
Weighing Precision	$\pm 0.01\%$
Resolution	$< 0.1\mu\text{g}$
Weight Baseline Drift	$< 10\mu\text{g}$

Table A.2: DSC2500 Instrument Specification

Temperature Accuracy	$\pm 0.025^{\circ}\text{C}$
Temperature Precision	$\pm 0.005^{\circ}\text{C}$
Enthalpy Precision	$\pm 0.04\%$
Baseline Flatness (-50-300°C)	$\leq 5\mu\text{W}$
Baseline Repeatability (-50-300°C)	$< 10\mu\text{W}$

REFERENCE LIST

- [1] Al-Absi, Z. A., Mohd Isa, M. H., and Ismail, M. Assessment of Building Façade Thermal Performance for the Potential Application of Phase Change Materials (PCMs) in Malaysia, a Case Study. In *ICACE 2019* (Singapore, 2020), M. Awang and M. R. Meor M Fared, Eds., Springer Singapore, pp. 129–141.
- [2] Alfaro-Ayala, J. A., Martinez-Rodriguez, G., Picon-Nunez, M., Uribe-Ramirez, A. R., and Gallegos-Munoz, A. Numerical study of a low temperature water-in-glass evacuated tube solar collector. *Energy Conversion and Management* 94 (2015), 472 – 481.
- [3] Alva, G., Liu, L., Huang, X., and Fang, G. Thermal energy storage materials and systems for solar energy applications. *Renewable and Sustainable Energy Reviews* 68 (2017), 693 – 706.
- [4] Anish, R., Mariappan, V., Joybari, M. M., and Abdulateef, A. M. Performance comparison of the thermal behavior of xylitol and erythritol in a double spiral coil latent heat storage system. *Thermal Science and Engineering Progress* 15 (2020), 100441.
- [5] Apricus. Ap Evacuated Tube Solar Collector 2013.

- [6] Barreneche, C., Navarro, M. E., Fernández, A. I., and Cabeza, L. F. Improvement of the thermal inertia of building materials incorporating PCM. Evaluation in the macroscale. *Applied Energy* 109 (2013), 428 – 432.
- [7] Bouhal, T., ed DÃ©n Fertahi, S., Agrouaz, Y., Rhafiki], T. E., Zeraouli, Y., and Jamil, A. Towards an energy efficiency optimization of solar horizontal storage tanks and circulation pipes integrating evacuated tube collectors through CFD parametric studies. *Sustainable Energy Technologies and Assessments* 26 (2018), 93 – 104.
- [8] Browne, M. C., Norton, B., and McCormack, S. J. Heat retention of a photovoltaic/thermal collector with PCM. *Solar Energy* 133 (2016), 533 – 548.
- [9] Cabeza, L., Castell, A., Barreneche, C., de Gracia, A., and Fernández, A. Materials used as PCM in thermal energy storage in buildings: A review. *Renewable and Sustainable Energy Reviews* 15, 3 (2011), 1675 – 1695.
- [10] Challa, G. R., Natarajan, M., and Palayakkodan, A. Experimental study on performance enhancement of evacuated tube by constant heat flux mode. *Applied Solar Energy* 54, 1 (2018), 40–49.
- [11] Chieruzzi, M., Cerritelli, G. F., Miliozzi, A., and Kenny, J. Effect of nanoparticles on heat capacity of nanofluids based on molten salts as PCM for thermal energy storage. *Nanoscale Research Letters* 8, 1 (2013), 448.

- [12] Coccia, G., Aquilanti, A., Tomassetti, S., Comodi, G., and Nicola, G. D. Design, realization, and tests of a portable solar box cooker coupled with an erythritol-based PCM thermal energy storage. *Solar Energy* 201 (2020), 530 – 540.
- [13] ed DÃ©n Fertahi, S., Bouhal, T., Kousksou, T., Jamil, A., and Benbassou, A. Experimental study and CFD thermal assessment of horizontal hot water storage tank integrating Evacuated Tube Collectors with heat pipes. *Solar Energy* 170 (2018), 234 – 251.
- [14] Essa, M. A., and Mostafa, N. H. Theoretical and experimental study for temperature distribution and flow profile in all water evacuated tube solar collector considering solar radiation boundary condition. *Solar Energy* 142 (2017), 267 – 277.
- [15] Farjallah, R., Chaabane, M., Mhiri, H., Bournot, P., and Dhaouadi, H. Thermal Performance of the U-Tube Solar Collector Using Computational Fluid Dynamics Simulation. *Journal of Solar Energy Engineering* 138, 6 (09 2016). 061008.
- [16] Fazilati, M. A., and Alemrajabi, A. A. Phase change material for enhancing solar water heater, an experimental approach. *Energy Conversion and Management* 71 (2013), 138 – 145.
- [17] Fernandez, A., Galleguillos, H., Fuentealba, E., and Perez, F. Thermal characterization of HITEC molten salt for energy storage in solar linear concentrated technology. *Journal of Thermal Analysis and Calorimetry* 122, 1 (2015), 3–9.

- [18] Fluent, A. ANSYS FLUENT 12.0 User's Guide. Tech. rep., Canonsburg, PA, USA, 2009.
- [19] Fluent, A. ANSYS Fluent UDF Manual. Tech. rep., Canonsburg, PA, USA, 2013.
- [20] Gao, Y., Fan, R., Zhang, X., AN, Y., Wang, M., Gao, Y., and Yu, Y. Thermal performance and parameter analysis of a U-pipe evacuated solar tube collector. *Solar Energy* 107 (2014), 714 – 727.
- [21] Guo, S., Liu, Q., Zhao, J., Jin, G., Wang, X., Lang, Z., He, W., and Gong, Z. Evaluation and comparison of erythritol-based composites with addition of expanded graphite and carbon nanotubes. *Applied Energy* 205 (2017), 703–709.
- [22] Hamdy, E., Ebrahim, S., Abulfotuh, F., and Soliman, M. Effect of multi-walled carbon nanotubes on thermal properties of nitrate molten salts. 317–320.
- [23] Hernandez-Perez, V., Abdulkadir, M., and Azzopardi, B. Grid Generation Issues in the CFD Modelling of Two-Phase Flow in a Pipe. *The Journal of Computational Multiphase Flows* 3, 1 (2011), 13–26.
- [24] Ho, M. X., and Pan, C. Optimal concentration of alumina nanoparticles in molten Hitec salt to maximize its specific heat capacity. *International Journal of Heat and Mass Transfer* 70 (2014), 174 – 184.
- [25] Hühlein, S., König-Haagen, A., and Brüggemann, D. Thermophysical characterization of $\text{MgCl}_2 \cdot 6\text{H}_2\text{O}$, xylitol and erythritol as phase change materials (PCM) for latent heat thermal energy storage (LHTES). *Materials* 10, 4 (2017), 444.

- [26] Hwang, Y., Park, H., Lee, J., and Jung, W. Thermal conductivity and lubrication characteristics of nanofluids. *Current Applied Physics* 6 (2006), e67–e71.
- [27] Iranmanesh, M., Akhijahani, H. S., and Jahromi, M. S. B. CFD modeling and evaluation the performance of a solar cabinet dryer equipped with evacuated tube solar collector and thermal storage system. *Renewable Energy* 145 (2020), 1192 – 1213.
- [28] Jing, B., Wang, Z., Tan, F., Guo, Y., Tong, S., Wang, W., Zhang, Y., and Ge, M. Hygroscopic behavior of atmospheric aerosols containing nitrate salts and water-soluble organic acids. *Atmospheric Chemistry & Physics* 18, 7 (2018).
- [29] Kaizawa, A., Kamano, H., Kawai, A., Jozuka, T., Senda, T., Maruoka, N., and Akiyama, T. Thermal and flow behaviors in heat transportation container using phase change material. *Energy Conversion and Management* 49, 4 (2008), 698 – 706.
- [30] Kalogirou, S. A. Solar thermal collectors and applications. *Progress in Energy and Combustion Science* 30, 3 (2004), 231 – 295.
- [31] Kaya, H., and Arslan, K. Numerical investigation of efficiency and economic analysis of an evacuated U-tube solar collector with different nanofluids. *Heat and Mass Transfer* 55, 3 (2019), 581–593.

- [32] Khan, M. M. A., Ibrahim, N. I., Mahbubul, I., Ali, H. M., Saidur, R., and Al-Sulaiman, F. A. Evaluation of solar collector designs with integrated latent heat thermal energy storage: A review. *Solar Energy* 166 (2018), 334 – 350.
- [33] Kholmanov, I., Kim, J., Ou, E., Ruoff, R. S., and Shi, L. Continuous Carbon Nanotube-Ultrathin Graphite Hybrid Foams for Increased Thermal Conductivity and Suppressed Subcooling in Composite Phase Change Materials. *ACS Nano* 9, 12 (2015), 11699–11707. PMID: 26529570.
- [34] Lim, C. S. L., Weaver, R., and Sobhansarbandi, S. Heat Transfer Enhancement of Phase Change Materials for Thermal Energy Storage Systems. V001T12A005.
- [35] Mangal, D., Lamba, D. K., Gupta, T., and Jhamb, K. Acknowledgement of evacuated tube solar water heater over flat plate solar water heater. *International Journal of Engineering (IJE)* 4, 4 (2010), 279.
- [36] Martin, P. CFD in the real world. *ASHRAE Journal* 41, 1 (01 1999), 20. Copyright - Copyright American Society of Heating, Refrigeration and Air Conditioning Engineers, Inc. Jan 1999; Last updated - 2012-04-04; CODEN - ASHRAA.
- [37] Nakano, K., Masuda, Y., and Daiguji, H. Crystallization and Melting Behavior of Erythritol In and Around Two-Dimensional Hexagonal Mesoporous Silica. *The Journal of Physical Chemistry C* 119, 9 (2015), 4769–4777.

- [38] Nomura, T., Tsubota, M., Oya, T., Okinaka, N., and Akiyama, T. Heat release performance of direct-contact heat exchanger with erythritol as phase change material. *Applied Thermal Engineering* 61, 2 (2013), 28 – 35.
- [39] Papadimitratos, A., Sobhansarbandi, S., Pozdin, V., Zakhidov, A., and Hassanipour, F. Evacuated tube solar collectors integrated with phase change materials. *Solar Energy* 129 (2016), 10 – 19.
- [40] Parth, V. Rheological Testing of Erythritol Samples. 2020.
- [41] Pawar, V. R., and Sobhansarbandi, S. CFD modeling of a thermal energy storage based heat pipe evacuated tube solar collector. *Journal of Energy Storage* 30 (2020), 101528.
- [42] Peng, Q., Wei, X., Ding, J., Yang, J., and Yang, X. High-temperature thermal stability of molten salt materials. *International Journal of Energy Research* 32, 12 (2008), 1164–1174.
- [43] Peng, X., Yao, M., Root, T. W., and Maravelias, C. T. Design and analysis of concentrating solar power plants with fixed-bed reactors for thermochemical energy storage. *Applied Energy* 262 (2020), 114543.
- [44] Qiu, S., Ruth, M., and Ghosh, S. Evacuated tube collectors: A notable driver behind the solar water heater industry in China. *Renewable and Sustainable Energy Reviews* 47 (2015), 580 – 588.

- [45] Sabiha, M., Saidur, R., Mekhilef, S., and Mahian, O. Progress and latest developments of evacuated tube solar collectors. *Renewable and Sustainable Energy Reviews* 51 (2015), 1038 – 1054.
- [46] Sakhrieh, A., and Al-Ghandoor, A. Experimental investigation of the performance of five types of solar collectors. *Energy Conversion and Management* 65 (2013), 715 – 720. Global Conference on Renewable energy and Energy Efficiency for Desert Regions 2011.
- [47] Saleel, C. A., Mujeebu, M. A., and Algarni, S. Coconut oil as phase change material to maintain thermal comfort in passenger vehicles. *Journal of Thermal Analysis and Calorimetry* 136, 2 (2019), 629–636.
- [48] Sari, A., Eroglu, R., Biçer, A., and Karaipekli, A. Synthesis and Thermal Energy Storage Properties of Erythritol Tetrastearate and Erythritol Tetrapalmitate. *Chemical Engineering & Technology* 34, 1 (2011), 87–92.
- [49] Serrano-López, R., Fradera, J., and Cuesta-López, S. Molten salts database for energy applications. *Chemical Engineering and Processing: Process Intensification* 73 (2013), 87–102.
- [50] Sharma, A., Tyagi, V., Chen, C., and Buddhi, D. Review on thermal energy storage with phase change materials and applications. *Renewable and Sustainable Energy Reviews* 13, 2 (2009), 318 – 345.

- [51] Sharma, S., Iwata, T., Kitano, H., and Sagara, K. Thermal performance of a solar cooker based on an evacuated tube solar collector with a PCM storage unit. *Solar Energy* 78, 3 (2005), 416 – 426.
- [52] Shen, S., Tan, S., Wu, S., Guo, C., Liang, J., Yang, Q., Xu, G., and Deng, J. The effects of modified carbon nanotubes on the thermal properties of erythritol as phase change materials. *Energy Conversion and Management* 157 (2018), 41 – 48.
- [53] Shin, D., and Banerjee, D. Enhancement of specific heat capacity of high-temperature silica-nanofluids synthesized in alkali chloride salt eutectics for solar thermal-energy storage applications. *International Journal of Heat and Mass Transfer* 54, 5 (2011), 1064 – 1070.
- [54] Sohal, M. S., Ebner, M. A., Sabharwall, P., and Sharpe, P. Engineering Database of Liquid Salt Thermophysical and Thermochemical Properties.
- [55] Souayfane, F., Fardoun, F., and Biwole, P.-H. Phase change materials (PCM) for cooling applications in buildings: A review. *Energy and Buildings* 129 (2016), 396 – 431.
- [56] Sundar, L. S., Ramana, E. V., Singh, M. K., and Sousa, A. C. Thermal conductivity and viscosity of stabilized ethylene glycol and water mixture Al₂O₃ nanofluids for heat transfer applications: An experimental study. *International Communications in Heat and Mass Transfer* 56 (2014), 86 – 95.
- [57] TAInstruments. Discovery DSC2500. Tech. rep., New Castle, DE, USA, 2018.

- [58] TAINstruments. Discovery TGA5500. Tech. rep., New Castle, DE, USA, 2018.
- [59] Thomas, L. C. Modulated DSC Paper 5, Measurement of Glass Transition and Enthalpic Recovery. Tech. rep., New Castle, DE, USA, 2005.
- [60] Touloukian, Y. S., Powell, R. W., Ho, C. Y., and Klemens, P. G. Thermophysical properties of matter - the TPRC data series. Volume 2. Thermal conductivity - nonmetallic solids. (Reannouncement). Data book.
- [61] Tyagi, V. V., and Buddhi, D. PCM thermal storage in buildings: A state of art. *Renewable and Sustainable Energy Reviews* 11, 6 (2007), 1146 – 1166.
- [62] Vignarooban, K., Xu, X., Arvay, A., Hsu, K., and Kannan, A. Heat transfer fluids for concentrating solar power systems – A review. *Applied Energy* 146 (2015), 383 – 396.
- [63] Wang, Y., Li, S., Zhang, T., Zhang, D., and Ji, H. Supercooling suppression and thermal behavior improvement of erythritol as phase change material for thermal energy storage. *Solar Energy Materials and Solar Cells* 171 (2017), 60 – 71.
- [64] Wang, Y., Wang, L., Xie, N., Lin, X., and Chen, H. Experimental study on the melting and solidification behavior of erythritol in a vertical shell-and-tube latent heat thermal storage unit. *International Journal of Heat and Mass Transfer* 99 (2016), 770 – 781.

- [65] Wu, Y., Li, J., Wang, M., Wang, H., Zhong, Y., Zhao, Y., Wei, M., and Li, Y. Solar salt doped by MWCNTs as a promising high thermal conductivity material for CSP. *RSC advances* 8, 34 (2018), 19251–19260.
- [66] Zeng, J., and Xuan, Y. Enhanced solar thermal conversion and thermal conduction of MWCNT-SiO₂/Ag binary nanofluids. *Applied Energy* 212 (2018), 809 – 819.
- [67] Zhichao, L., Qiang, Z., and Gaohui, W. Preparation and enhanced heat capacity of nano-titania doped erythritol as phase change material. *International Journal of Heat and Mass Transfer* 80 (2015), 653–659.

VITA

Celine S.L. Lim was born on July 5, 1996 in Selangor, Malaysia. She grew up in Shah Alam city and attended high school at Sekolah Menengah Kebangsaan USJ 12. After graduating high school, she started college at Missouri Western State University pursuing an engineering technology degree before transferring to University of Missouri - Kansas City where she received her bachelor's in Mechanical Engineering. Aside from academics, Celine was also heavily involved as a student-athlete for the UMKC women's golf team and have represented the university to compete in multiple golf tournaments. Celine started her research work in the Renewable Energy Research Lab in July 2018 during her senior year. As an undergraduate, Celine was awarded the UMKC SEARCH grant and was chosen to represent UMKC for Undergrad Research Day at the Capitol. She also presented her research work at the 2019 ASME Power conference and has won the Best Paper Award in the student competition track. While as a Master's student, Celine was also awarded the UMKC Graduate Assistant (GAF) fellowship and was named 2020 Outstanding Master Student of Mechanical Engineering. Upon her graduation, she plans to continue to pursue her Ph.D at UMKC.